Commissioning of a 4D MRI phantom for use in MR-guided radiotherapy

Schneider, S.; Dolde, K.; Engler, J.; Hoffmann, A.; Pfaffenberger, A.;

Originally published:

October 2018

Medical Physics 46(2019)1, 25-33

DOI: https://doi.org/10.1002/mp.13261

Commissioning of a 4D MRI phantom for use in MR-guided radiotherapy

Kai Dolde[1,2,3,*,†], Sergej Schneider[4,5,†], Johanna Engler[5], Asja Pfaffenberger[1,2,§], Aswin Hoffmann[4,5,6,§]

[1] *German Cancer Research Center (DKFZ), Medical Physics in Radiotherapy, Heidelberg, Germany*

[2] *National Center for Radiation Research in Oncology, Heidelberg Institute for Radiooncology, Heidelberg, Germany*

[3] *University of Heidelberg, Department of Physics and Astronomy, Heidelberg, Germany*

[4] *Institute of Radiooncology – OncoRay, Helmholtz-Zentrum Dresden-Rossendorf, Dresden, Germany*

[5] *OncoRay – National Center for Radiation Research in Oncology, Faculty of Medicine and University Hospital Carl Gustav Carus, Technische Universität Dresden, Helmholtz-Zentrum Dresden-Rossendorf, Dresden, Germany*

[6] *Department of Radiotherapy and Radiation Oncology, Faculty of Medicine and University Hospital Carl Gustav Carus, Technische Universität Dresden, Dresden, Germany*

[†]Both authors contributed equally.

[§]Both authors contributed equally.

[*]Corresponding author:
Kai Dolde, MSc
German Cancer Research Center (DKFZ), Medical Physics in Radiation Oncology, Heidelberg, Germany
Im Neuenheimer Feld 280
69120 Heidelberg, Germany
E-Mail: k.dolde@dkfz.de

Number of Pages : 19
Number of Figures : 8
Number of Tables : 6
Number of supplementary Tables : 0
Number of supplementary Figures : 0

Running Head: Commissioning of 4D MRI phantom

Key words: MRI, dynamic phantom, image-guided radiation therapy, commissioning

ABSTRACT

Purpose:

Systems for integrated magnetic resonance guided radiation therapy (MRgRT) provide real-time and on-line MRI guidance for unequalled targeting performance of moving tumors and organs at risk. The clinical introduction of such systems requires dedicated methods for commissioning and routine machine quality assurance (QA). The aim of the study was to develop a commissioning protocol and method for automatic quantification of target motion and geometric accuracy using a 4D MRI motion phantom.

Material and Methods:

The commissioning was performed on a clinically used 3T MR scanner. The phantom was positioned on a flat tabletop overlay using an in-house constructed base plate for a quick and reproducible setup. The torso-shaped phantom body, which was filled with mineral oil as signal generating medium, includes a 3D grid structure for image distortion analysis and a cylindrical thru-hole in which a software-controlled moving rod with a hypo-intense background gel and a decentralized hyper-intense target simulates 3D organ motion patterns. To allow for sequence optimization, MR relaxometry was performed to determine the longitudinal T_1 and transverse T_2 relaxation times of both target and background gel in the movable cylinder. The geometric image distortion was determined as the mean and maximum 3D Euclidean distance (Δ_{mean}, Δ_{max}) of grid points determined by non-rigid registration of a 3D spoiled gradient echo MRI scan and a CT scan. Sinusoidal 1D/2D/3D motion trajectories, varying in amplitude and frequency, as well as an exemplary 1D MR-navigator diaphragm motion pattern extracted from a volunteer scan were scanned by means of 2D cine MRI. Target positions were automatically extracted from 2D cine MRI using an in-house developed software tool.

Results:

The base plate enabled a reproducible setup with a deviation of <1 mm in all directions. Relaxometry yielded T_1/T_2 values for target and background gel of 208.1 ± 2.8 / 30.5 ± 4.7 ms and 871 ± 36 / 13.4 ± 1.3 ms respectively. The geometric distortion in the MRI scan increased with distance from the magnetic isocenter,

with Δ_{mean}=0.58±0.30 mm and Δ_{max}=1.31 mm. The frequencies of the reconstructed motion patterns agreed with the pre-set values within 0.5%, whereas the reconstructed amplitudes showed a maximum deviation to the pre-set amplitudes of <0.4 mm in AP/LR direction and <0.2 mm in IS direction.

Conclusion:

A method and protocol for commissioning of a 4D MRI motion phantom on a 3T MR scanner for MRgRT was developed. High-contrast and geometrically reliable 2D cine MR images of the phantom's moving target could be obtained. The pre-set motion parameters could be extracted with sufficient spatio-temporal accuracy from 2D cine MRI in all motion directions. The measured geometric image distortion of <1.31mm within the phantom grid confirms geometric accuracy of the clinically utilized 3D spoiled gradient echo sequence.

The method developed can be used for routine QA tests of spatio-temporally resolved MRI data in MRgRT.

1. Introduction

To increase the accuracy of radiation therapy (RT) for patients with moving tumors, it is of paramount importance to take intrafractional motion into account during pre-treatment image acquisition, treatment planning and dose delivery [1]. Intrafractional motion involves physiologic processes that have its origin in respiratory, cardiac, muscular and gastrointestinal (e.g. organ filling and peristalsis) systems. Respiratory motion is the predominant cause of motion affecting all tumor sites in the thorax, abdomen and pelvis. The quantification and management of respiratory motion is therefore an essential component to improve treatment outcome through image-guided radiotherapy.

The excellent soft-tissue contrast and absence of ionizing radiation of magnetic resonance imaging (MRI), makes MRI a promising imaging modality for quantification of tumor motion. To accurately account for the motion of tumors and surrounding organs during radiation delivery, hybrid MR-LINAC devices have been developed [2-5], which integrate an MR-scanner with a linear accelerator (LINAC) for real-time MR-guided radiation therapy (MRgRT). These hybrid systems allow for real-time MRI-based gating and motion tracking. For the commissioning of such systems, the accuracy and precision of motion tracking through MRI needs to be assessed and dedicated pulse sequences for cine MRI need to be examined in a quality assurance (QA) procedure.

For this purpose, dynamic motion phantoms are used to simulate and observe reproducible motion patterns and extract ground-truth images, which are generally not available for patients due to day-to-day variations in patient geometry, breathing patterns and uncertainties in patient positioning. MR-compatible motion phantoms have been developed in the past years [6, 7], and mainly consist of an inner rotatable and outer rigid cylinder, a design principle that is still common for different motion phantoms nowadays. Several institutions have been working on 1D/2D motion phantoms to validate motion in MR images, e.g. [8-10]. Today, different programmable commercial 3D motion phantoms are available to validate motion patterns in all three spatial dimensions to be used as QA devices, like the MRI-LINAC Dynamic Phantom (Model 008M, Computerized Imaging Reference Systems Inc., Norfolk, USA). This phantom has already been investigated regarding static geometric distortions [11] but to fully exploit its features for MRgRT, a comprehensive commissioning is essential including an analysis of setup reproducibility, precision of motion extraction, MR relaxation properties as well as geometric distortions. It is the aim of this study to develop a

commissioning protocol and method for automatic quantification of target motion and geometric distortion for the MRI-LINAC Dynamic Phantom that is also applicable to other 4D MR motion phantoms.

2. Material and Methods

2.1. 4D MRI Phantom

Fig. 1. Schematic setup of the MRI-LINAC Dynamic Phantom [12] comprising an actuator [left], modular extension shafts [middle], and movable cylinder with simulated target inserted into a torso-shaped body [right].

The 4D MRI motion phantom [12] consists of a shell body approximating a human torso in size and shape (25.5 × 29.5 × 20 cm³). The shell can be filled by the user with an MR signal generating fluid, which in this study was 7.6l of mineral oil (Marcol Blend 3T, Philips Healthcare), resulting in a total phantom mass of 12kg. The phantom includes a 3D distortion grid for the assessment of geometric accuracy as well as a central fiducial aligned with exterior laser marks on the shell body to facilitate a laser-to-isocenter coincidence analysis. A cylindrical thru-hole is incorporated in the phantom body to accommodate a cylinder with a decentralized hyper-intense target gel to perform rotational and translational movements. The 3D target motion is software-controlled by an MR-conditional actuator positioned at a distance of up to 2.655 m to the phantom through the connection of modular extendable rigid shafts (Figure 1). The target can optionally host MR-compatible dosimeters for treatment dose verification.

2.2. Positioning Setup

The phantom was commissioned on a 3T MRI scanner (Achieva 3.0T, Philips Healthcare, Cleveland, USA) using a 32-channel SENSE Torso/Cardiac coil. The posterior coil was positioned underneath a glass-fiber flat tabletop overlay with a coil holder (Medibord Ltd, Nottingham, UK), which enabled a stable positioning

of the phantom on the patient couch. The distance of 2.655 m between the actuator and magnetic isocenter of the MRI scanner bore, as advised by the phantom manufacturer, could not be realized on the patient couch, which only allowed for a maximum distance of 1.65 m relative to the magnetic isocenter. This provided a safety margin of only 15 cm to the 0.2 T field contour of the MRI scanner, which was stated as the minimum distance by the phantom manufacturer. Hence, a base plate for the actuator made of polyvinyl chloride (PVC) and polyurethane (PUR) was constructed to both extend the couch by 30 cm as well as to mechanically fix the actuator to the couch and avoid any projectile hazard in case the 0.2 T field contour is exceeded by a user-related positioning error. Additionally, a base plate made out of poly methyl methacrylate (PMMA) was constructed to allow fast and accurate positioning of the phantom body onto the patient couch (Figure 2).

Fig. 2. Left: setup of 4D MRI phantom on flat tabletop overlay positioned on the patient couch. Top right: close-up view of phantom positioned on base plate. Bottom right: close-up view of actuator positioned on base plate couch extension.

2.3 Target relaxometry

For pulse sequence optimization purposes and an elaborated choice of signal generating medium the longitudinal (T_1) and transverse (T_2) relaxation times of the target and background gels in the cylinder were determined by MR relaxometry. To this end, the movable cylinder was scanned using an 8-channel SENSE head coil. For T_1 determination MR relaxometry was performed with an inversion recovery spin-echo (IR SE) method with six different inversion times (TI). A T_1-map was calculated by fitting the complex data to a five-parameter model [13]. A T_2-map was calculated based on a gradient-and-spin-echo (GraSE) sequence

[14] sampled at nine echo times (TE) by fitting the magnitude data to a mono-exponential function. To minimize the influence of B_1 inhomogeneities found in multi-echo SE sequences a correction was performed by discarding the first echo signal [15, 16]. The scan parameters used for MR relaxometry are summarized in Table 1.

Table 1. Scan parameters used for MR relaxometry to determine the longitudinal (T_1) and transverse (T_2) relaxation times of both the target and background gel in the movable cylinder of the phantom.

Sequence	Resolution [mm²]	Slice thickness [mm]	FOV [mm³]	BW [Hz/voxel]	TE/TR [ms]	TI [ms]	ΔTE [ms]
IR SE for T_1 mapping	1.56×1.56	5	150×150×50	2378	26/5000	50/150/500/ 900/1500/3400	-
GraSE for T_2 mapping	1.0×1.0	6	150×150×6	2331	8.6/5000	-	8.6

Abbreviations: FOV = field of view, BW = bandwidth, TE = echo time; TR = repetition time, TI = inversion time, ΔTE = difference in echo time.

2.4. Distortion grid and laser-to-central fiducial alignment

A computed tomography (CT) scan of the phantom was acquired (Somatom Definition AS, Siemens Healthineers, Erlangen, Germany) as the ground truth for assessment of the geometric distortion in MRI. A 3D gradient echo (GRE) sequence (THRIVE) was used which is clinically relevant for abdominal imaging. The scan parameters used for CT and MR imaging of the 3D grid are summarized in Table 2, where the MR scan was acquired in transverse orientation with phase encoding in anterior-posterior direction.

Since the used MR scanner only allows for a laser alignment along the longitudinal axis, the phantom was positioned differently along the sagittal axis relative to the isocenter of the CT and MR scanner, respectively. Furthermore, since the custom made positioning setup was only applicable for the patient couch of the MR scanner, user related positioning errors are expected in both the form of translation as well as rotation in coronal plane. These positioning differences have to be corrected for by rigid registration in order to solely analyze image distortion in MRI. Both the correction by rigid registration as well as the final non-rigid registration for distortion analysis was performed with the open source software *elastix* [17, 18].

In order to correct the discrepancy due to patients couch height and lateral translation, a rigid registration was performed based on the grid point closest to the magnetic isocenter (see Fig. 4). For longitudinal translation correction, the central fiducial was used as reference point. Furthermore, an Euler transformation was performed to correct for rotational differences of the phantom in coronal plane on the scanners patient couch. For the non-rigid registration a binary mask was applied onto the CT scan to exclude the phantoms PMMA shell, which is not visible in MRI. Non-rigid registration was performed, utilizing the transformation functions "AffineTransform" and "BSplineTransform". The geometric distortion was derived from the transformation as the mean and maximum 3D Euclidean distance (Δ_{mean}, Δ_{max}) between identical grid points in MRI and CT , respectively. The 3D distortion hence includes the in-plane distortion of all three planes.

In order to test the reproducibility of the laser-to-central fiducial alignment with the custom-made setup, the phantom was scanned twice with MRI while centering the grid in the isocenter, and the center-of-mass position of the central fiducial was compared between both.

Table 2. Scan parameters used for MR and CT image acquisition of the 3D distortion grid and evaluation of the setup reproducibility.

Modality	Resolution [mm²]	Slice thickness [mm]	FOV [mm³]	BW [Hz/voxel]	TE/TR [ms]	Tube voltage [kVp]	Tube current time product [mAs]
MRI	1.47×1.47	1.5	352×240×200	721	1.4/3	-	-
CT	0.68×0.68	0.6	350×350×315	-	-	80	420

Abbreviations: FOV = field of view, BW = bandwidth, TE = echo time; TR = repetition time.

2.5 Target motion evaluation

Balanced turbo field-echo (bTFE) sequences based on balanced steady-state free precession techniques provide rapid and high signal-to-noise MR images, and therefore are successfully applied for fast 2D cine MRI [19,20]. A bTFE sequence was used for the evaluation of 1D- and 2D-motion trajectories in single-slice coronal and transverse 2D cine MRI. For the analysis of 3D-motion trajectories, an orthogonal 2D cine MRI scan was acquired interleaved in transverse and sagittal orientation. All cine MR images were acquired with a temporal resolution of 0.5–0.7 s.

Sinusoidal 1D-, 2D- and 3D-motion trajectories were programmed in the graphical user interface of the target motion control software. The pre-set frequencies and amplitudes were based on breathing patterns typically observed in patients (0.1–0.2 Hz) [1]. The maximum amplitude was limited by the phantom design to be ±25/±5/±5 mm in inferior-superior (IS) /anterior-posterior (AP)/left-right(LR) direction. In addition, a realistic motion pattern was imported from a 1D MR navigator acquisition of a healthy volunteer with a mean frequency of 0.17 Hz and motion amplitudes < 20 mm

The motion analysis was performed using an in-house developed automated tracking algorithm based on functions provided by the Image Processing Toolbox from MATLAB (MATLAB R2016a, The Mathworks Inc., Natick, USA). The 2D cine MR images were first pre-processed by applying a Gaussian filter to reduce influence of noise and artifacts. Objects with connected structures were identified by threshold detection. From these objects, the target was identified by its known geometric properties. Subsequently, the center-of-mass of the target was determined as a surrogate for its position at each time step. The measured positions were fit with a sinusoidal function by minimizing squared errors using the simplex search method [21], from which the amplitude and frequency were estimated.

In order to verify the accuracy of the set target displacement of the phantom and to acquire ground truth images, a CT scan of the phantom was acquired in static maximum target displacement used for this study, with ±20/±5/±5 mm in IS/AP/LR direction. The pre-set values were then compared to the displacement of targets center-of-mass found in the CT scan. The CT and MR scan parameters are listed in Table 3.

Table 3. Scan parameters used in MR and CT imaging for target motion characterization. For 3D motion the 2D cine MRI was acquired interleaved in transverse and sagittal orientation.

Parameter	2D cine (1D motion)	2D cine (2D motion)	2D cine (3D motion)	CT (static 3D displacement)
Resolution [mm²]	1.34×1.34	1.34×1.34	1.34×1.34	0.68×0.68
Slice thickness [mm]	7	7	7	0.6
FOV [mm³]	300×300×7	300×300×7	300×300×7	350×350×315
BW [Hz/voxel]	1944	1944	1591	-
TE/TR [ms]	1.11/2.22	1.11/2.22	1.16/2.31	-
FA [°]	30	30	30	-
SENSE factor	1	1	1.5	-
Temporal resolution [s]	0.489	0.489	0.680	-

Tube voltage [kV]	-	-	-	80
Tube current [mA]	-	-	-	420

Abbreviations: FOV = field of view, BW = bandwidth, TE = echo time; TR = repetition time, FA = flip angle.

3. Results

3.1 MR relaxometry of target and background gels

MR relaxometry resulted in the quantitative T_1- and T_2-maps shown in Figure 3, from which it can be appreciated that the target and background gel in the movable cylinder show a different relaxation behavior at 3.0 T. The T_1 and T_2 relaxation times of both gels, determined as mean values over a manually defined region of interest of Figure 3, are listed in Table 4.

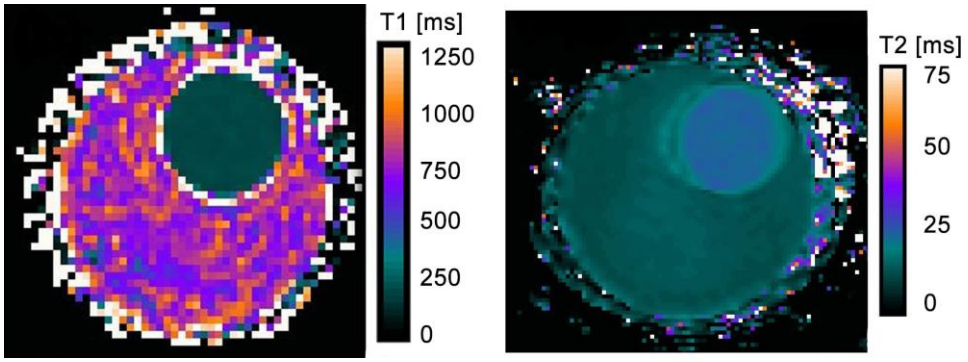

Fig. 3. Transversal maps of T_1 (left) and T_2 (right) relaxation times at 3T clearly show the decentralized target in the top right of the moving cylinder.

Table 4. Estimated (mean ± standard deviation) T_1 and T_2 relaxation times of the target and background gel in the movable cylinder as determined by 3.0 T MR relaxometry.

Structure	T_1 [ms]	T_2 [ms]
Target gel	208.1 ± 2.8	30.5±0.7
Background gel	871.0 ± 36.0	13.4±1.3

3.2. Distortion grid and positional reproducibility

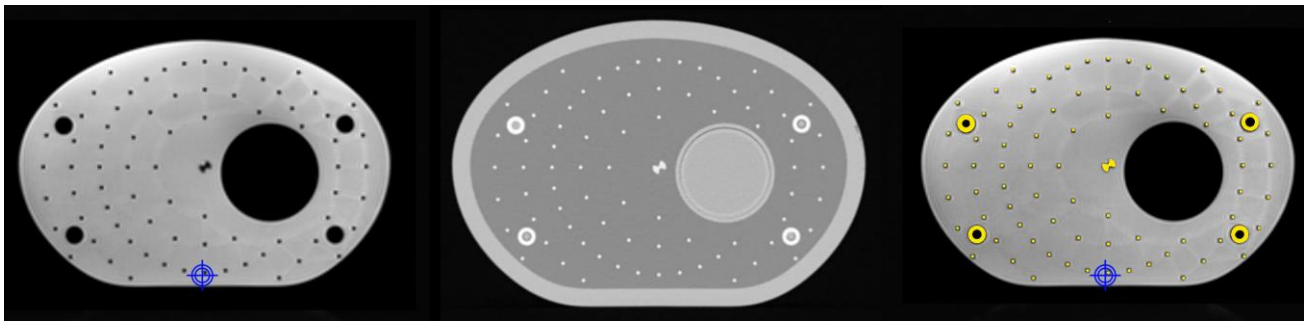

Fig. 4. Transverse MR (3D T1 GRE) [left] and CT [middle] image of the 3D distortion grid. For visualization the grid structure (yellow) was threshold segmented (155HU) in CT and registered with the MR image based on the grid point closest to the magnetic isocenter, (blue target) [right].

Figure 4 shows a transverse MR image (3D T1 GRE sequence) and a reference CT image of the 3D distortion grid at the same slice position which where rigidly registered after threshold segmentation [155 HU] of the grid in CT. The magnetic isocenter in the MR images was marked with a blue target. In Figure 5, the transverse geometric distortion is shown for 4 different slices of the grid. The MR images showed an increasing distortion with increasing distance to the magnetic isocenter (see figure 6)with Δ_{max} = 1.31 mm. The mean absolute 3D Euclidean distance between the grid points on MR and CT images measured over the whole grid volume was Δ_{mean} = 0.58 ± 0.30 mm.

The base plate positioning system was constructed with manufacturing tolerances <1 mm. An analysis of the setup reproducibility showed a positioning accuracy of <0.2 mm and 1 mm in transverse and longitudinal direction, respectively.

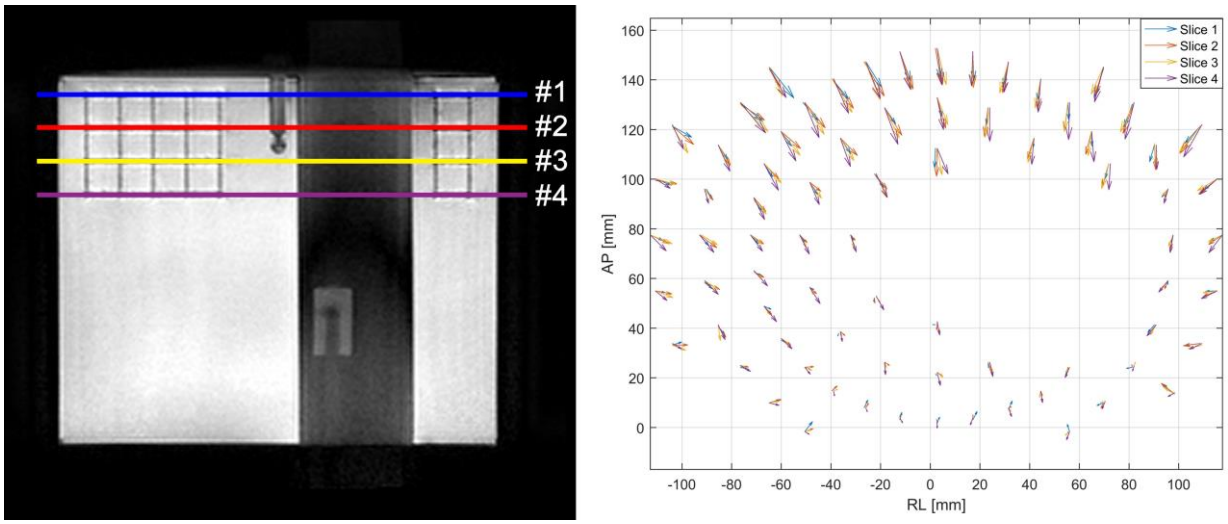

Fig. 5. Left: coronal MR image of the phantom with 4 transverse slices (color coded) at longitudinal distances to the central fiducial of z= [+30, +10, -10, -30] mm used for the geometric distortion analysis. Right: measured transverse geometric distortion between CT and MRI. The arrows were elongated by 10x for better visibility.

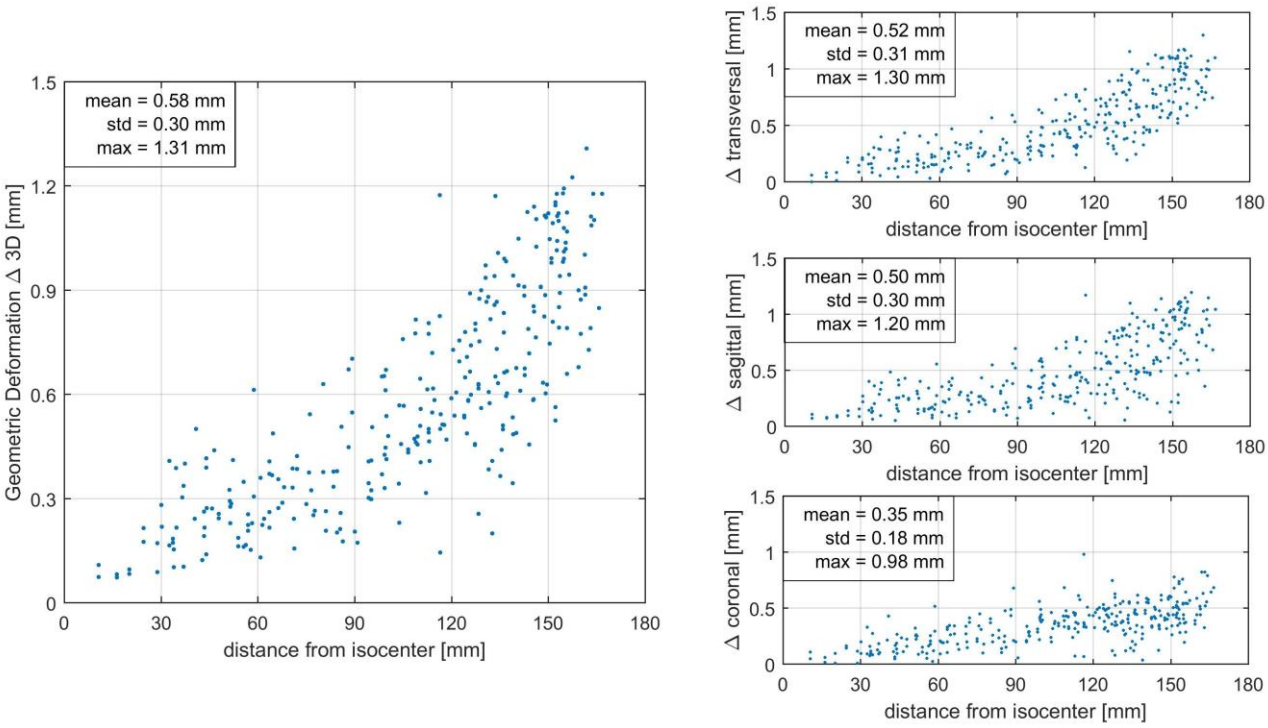

Fig. 6. Geometric deformation Δ, measured by non-rigid registration of the GRE MR image onto the reference CT in 3D [left], as well as 2D component of distortion in same sequence in transverse, sagittal and coronal orientation, respectively [right].

3.1. Static 3D displacement extracted from CT imaging

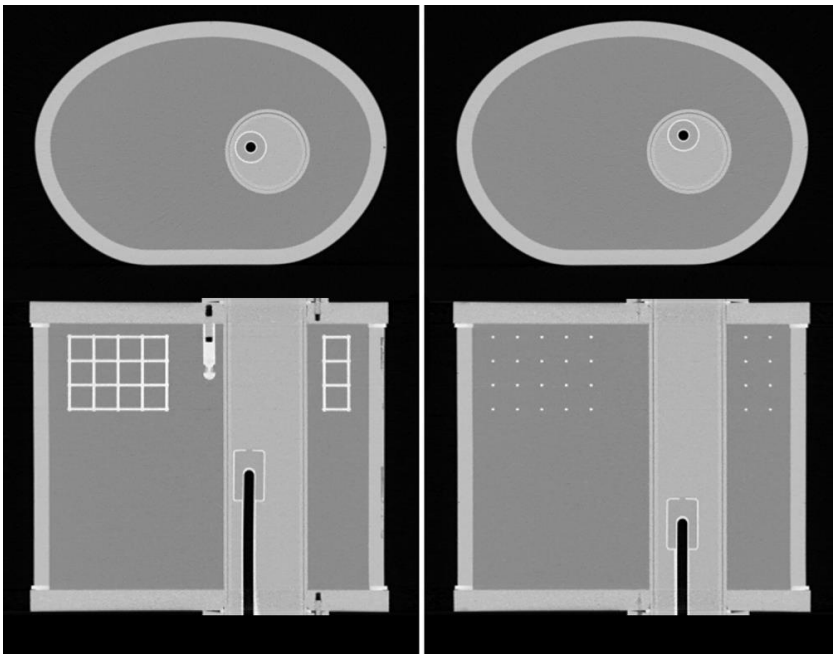

Fig. 7: Transverse [top] and reconstructed coronal [bottom] CT image of the phantom, using two extreme target positions: -20/-5/-5mm in IS/AP/LR [left] and +20/+5/+5mm in IS/AP/LR [right].

An exemplary transverse and coronal slice of the CT scan of the phantom is shown in Figure 6 where the maximum static target 3D displacement is clearly visible. The set target displacement and the measured displacement based on the center-of-mass of the target are summarized in Table 5. While in IS direction no deviation from the set displacement could be measured, the target showed a smaller displacement in AP/LR direction than defined in the controlling software.

Table 5. Comparison of pre-set target displacement to CT measurement between two different target positions.

Direction of displacement	Pre-set displacement [mm]	Measured displacement [mm]
IS	40.0	40.0
AP	10.0	9.6
LR	10.0	8.9

3.2. Motion parameters extracted from cine MRI

The motion trajectories programmed in the target motion control software and the motion patterns measured from 2D cine MRI are listed in Table 6. For the sinusoidal motion patterns, the estimated frequencies agreed

within 0.5% to the programmed frequencies. The measured amplitudes showed a maximum deviation <0.5 mm and 0.2 mm in AP/LR and IS direction, respectively. For the 1D navigator based motion pattern, the estimated motion parameters showed a maximum deviation in amplitude of 1.0 mm and a mean deviation of 0.3 mm in IS direction (Figure 7).

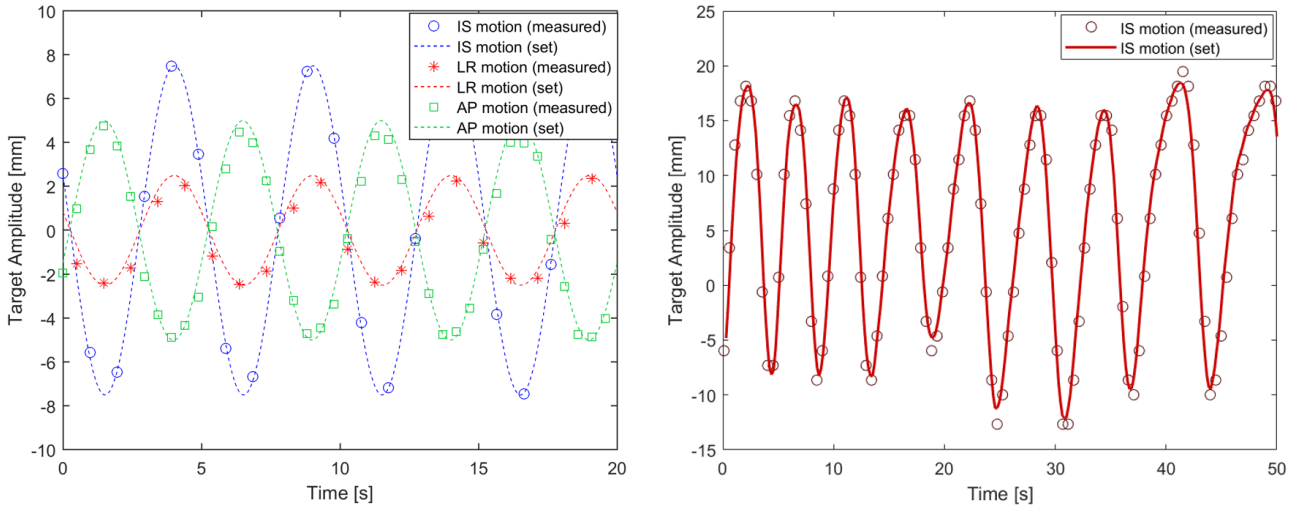

Fig. 8. Left: programmed and measured 3D sinusoidal target motion patterns using pre-set amplitudes of 7.5/5/2.5 mm in IS/AP/LR direction. Right: 1D navigator-based volunteer breathing pattern with pre-set and measured target positions.

Table 6. Comparison of pre-set and measured sinusoidal motion parameters.

Set parameters				Measured parameters			
IS amplitude [mm]	AP amplitude [mm]	LR amplitude [mm]	Frequency [Hz]	IS amplitude [mm]	AP amplitude [mm]	LR amplitude [mm]	Frequency [Hz]
20.0	0.0	0.0	0.2	20.2	-	0.2	0.199
10.0	0.0	0.0	0.2	10.1	-	0.0	0.199
20.0	0.0	0.0	0.1	20.2	-	0.1	0.100
0.0	5.0	0.0	0.2	-	4.6	0.4	0.199
0.0	0.0	5.0	0.2	-	0.5	4.6	0.199
20.0	5.0	0.0	0.2	20.1	4.6	-	0.199
20.0	0.0	5.0	0.2	20.1	-	4.7	0.199
0.0	5.0	5.0	0.2	-	4.8	4.7	0.199
7.5	5.0	2.5	0.2	7.5	4.7	2.3	0.200

Due to the underlying rotation of the target cylinder it appeared to be not possible to set a pure 1D motion in the transverse (AP/LR) plane. Therefore, a sole AP motion trajectory showed an additional displacement of

0.4 mm in LR direction, whereas a pure LR motion trajectory resulted in an additional displacement of 0.5 mm in AP direction.

4. Discussion

A protocol and method for commissioning of a 4D MRI dynamic phantom on a clinical 3T MRI scanner has been developed. The method for automatic quantification of 3D target motion by 2D cine MRI can be used for quality assurance of spatio-temporally resolved MR sequences used for MRgRT.

Before routine usage of the phantom on the designated MRI scanner, several setup issues had to be resolved. The flat tabletop overlay enabling to scan patients in radiation treatment position on the MR scanner's standard concave shaped patient couch allowed the usage of a coil holder to position a posterior torso/cardiac coil underneath the tabletop overlay. The coil holder setup ensures a stable positioning of the phantom directly on the flat tabletop. Furthermore, reproducible positioning of the phantom body based on the laser marks showed to be laborious due to the large mass of the phantom (12kg). Therefore an easily mountable base plate for the phantom was constructed to facilitate a fast and reproducible positioning of <1 mm without affecting MR image quality.

MR acquisitions with and without the actuator showed no effect on the image quality when positioning the actuator close to the 0.2 T field contour, stated as the minimum distance by the phantom manufacturer. However, at this position magnetic forces acting on the partially ferromagnetic actuator had to be considered. The limited length of the MR scanner's patient couch allowed a positioning of the actuator with a distance of maximum 1.65m from the magnetic isocenter, i.e. at a safety margin of only 15 cm to the 0.2 T field contour. An in-house developed fixation setup increased the safety margin by 30 cm and fixed the actuator on the couch to avoid any projectile hazard in case of accidental mispositioning of the phantom by the user.

MR relaxometry was performed to facilitate sequence optimization, i.e. adaption of the flip angle for contrast enhancement of the target. The relaxation parameters should also be considered for an elaborated choice of signal generating medium for the phantom body. For a different field strength than 3T the image quality needs to be reassessed and MR sequence parameters may need to be adjusted based on the T_1/T_2 values of target and background material to obtain high quality images.

In [11] an analysis of the 3D grid distortion on an identical MR scanner by means of different MR sequences (2D T1W FFE, 2D T1W TSE and 3D T1W TFE) has shown maximum deviations of 1.0, 0.7 and 1.8 mm, respectively. In the referenced study, however, distortion was considered only separately in lateral, anterior-posterior and cranio-caudal direction. In contrast in the present study, 3D distortion was analyzed based on the distortion grid and showed a sufficiently high geometric accuracy with an image distortion <1.31 mm over 32 cm diameter cylindrical volume (height = 6 cm) around the magnetic isocenter using the 3D GRE (THRIVE) sequence. With a distortion <1 mm within a radius of 130 mm to the magnetic isocenter the investigated sequence largely fulfills the criteria for stereotactic radiotherapy. It is, however, important to note that the investigated geometric distortion almost solely arises from system related field inhomogeneities or gradient non linearities. The additional patient related susceptibility induced geometric distortion was not included in the analysis. Furthermore, distortion was only analyzed for one clinically relevant sequence with a fixed bandwidth BW = 721 Hz/voxel. Since geometric distortion inversely correlates with bandwidth, sequences with other parameters will lead to different distortions.

The phantom's 3D grid covers a range of 6 cm in IS direction, which is sufficient for covering the maximum possible target motion of this phantom. The 3D grid is however not an adequate replacement of a large field homogeneity phantom in order to fully describe the magnetic field homogeneity. For this purpose, different 2D/3D grid-based MR phantoms like the ACR phantom [22] or large FOV field homogeneity phantoms [23,24] are available and have proven to be suitable for analysis of geometric distortions.

The measured motion parameters found in MRI agreed well with the pre-set values. The measured deviations in IS direction were <0.2 mm, in AP/LR slightly larger deviations of < 0.4 mm were found. MR motion analysis measurements with different MR motion phantoms have shown similar results with motion amplitude errors of 0.1–0.4 mm [2] and have reported on good agreement between measured and reference positions [25]. Similarly the reference CT measurement of the maximum static displacement showed a good agreement with the pre-set parameters, however not within the accuracy of < 0.1mm as stated by the vendor. While in IS direction no measurable deviation from the set amplitude was found, in AP/LR the target displacement was 0.2 mm and 0.5 mm, respectively. When considering this as intrinsic deviation of the phantom, the motion amplitude errors found in 2D cine MRI are within 0.2 mm in all directions.

With respect to motion extraction in MRgRT the 4D MR phantom used in this study shows some limitations. Firstly, the phantom motion is purely rigid, which is usually not the case for movable tumors or organs at risk. Secondly, for patient cases, image artifacts caused by different magnetic susceptibility may occur, leading to additional magnetic field distortions of the resulting MR images [26]. Future studies may take these effects into account by combination of measurements with both rigid phantoms with highly reproducible motion behaviors and dynamic non-rigid anthropomorphic phantoms [27, 28], which however may not fulfill a sub-mm motion precision.

The commissioning protocol for the CIRS MR-LINAC phantom proposed and presented in this study may also be applicable for other MR motion phantoms.

5. Conclusions

A method and protocol for commissioning a 4D MR dynamic motion phantom on a 3T MR scanner has been developed. It was shown that automatic localization of a moving target in 3D is feasible with high spatial and temporal accuracy through 2D cine MRI. The analysis of geometric distortion found in the 3D GRE TFE (THRIVE) sequence based on the 3D distortion grid revealed distortions within 1.31 mm, confirming a high geometric accuracy of this clinically relevant sequence.

Acknowledgment

The authors would like to thank Dr. M. Schürer and G. Rothe for their craftsmanship and help during the construction of the phantom and actuator base plate. We furthermore would like to thank P. Wohlfahrt and N. Peters for their support in imaging with CT.

Disclosure of Conflicts of Interest

No potential conflict of interest was reported by the authors.

References

[1] Keall P, Mageras G, Balter J, et al. The management of respiratory motion in radiation oncology report of AAPM Task Group 76. *Med. Phys*. 2006:33(10):3874-900
[2] Lagendijk JJW, Raaymakers BW, Raaijmakers AJE, et al. MRI/linac integration. *Radiother.Oncol.* 2008:86(1):25-9.
[3] Mutic S, Dempsey JF. The ViewRay system: magnetic resonance-guided and controlled radiotherapy. *Semin Radiat Oncol*. 2014:24(3):196-9.
[4] Fallone BG. The rotating biplanar linac-magnetic resonance imaging system. *Semin Radiat Oncol*. 2014:24(3): 200-2.
[5] Keall PJ, Barton M, Crozier S. The Australian magnetic resonance imaging-linac program. *Semin Radiat Oncol.* 2014:24(3):203-6.
[6] Young AA, Axel L. Validation of tagging with MR imaging to estimate material deformation. *Radiology*:1993:188(1):101-8.
[7] Drangova M, Bowman B. Physiologic motion phantom for MRI applications. *J Magn Reson Imaging*. 1996:6(3):513-8.
[8] Yue Y, Fan Z, Yang W, et al. Geometric validation of self-gating k-space-sorted 4D-MRI vs 4D-CT using a respiratory motion phantom. *Med Phys*. 2015:42(10):5787-97.
[9] Han F, Zhou Z. Respiratory motion-resolved, self-gated 4D-MRI using rotating cartesian k-space (ROCK). *Med Phys*. 2017:44(4):1359-68.
[10] Sagias G, Yiallouras C. An MRI-conditional motion phantom for the evaluation of high-intensity focused ultrasound protocols. *Int J Med Robot*. 2016:12(3):431-41.
[11] Fatemir-Ardekani A, Wronski M. SU-E-J-209: Geometric Distortion at 3T in a Commercial 4D MRI-Compatible Phantom. *Med Phys*. 2015:42(6):3313.
[12] CIRS, Computerized Imaging Reference Systems, Inc., Norfolk, Virginia USA.
[13] Barral JK, Gudmundson E. A robust methodology for in vivo T1 mapping. *Magn Reson Med*. 2010:64(4):1057-67.
[14] Fernández-Jiménez R, Sánchez-Gonzáles J, Aguero J, etl al. Fast T2 gradient-spin-echo (T2-GraSE) mapping for myocardial edema quantification: first in vivo validation in a porcine model of ischemia/reperfusion. *J Cardiovasc Magn Reson*. 2015:17:92
[15] Milford D, Rosbach N. Mono-Exponential Fitting in T2-Relaxometry: Relevance of Offset and First Echo. *PLos One*. 2015:10(12):e0145255.
[16] Lebel RM, Wilman AH. Transverse Relaxometry with Stimulated Echo Compensation. *Magn Reson Med.* 2010:64(4):1005-14.
[17] Klein S, Staring M, Murphy K, Viergever MA, Pluim JPW. Elastix: a toolbox for intensity based medical image registration. *IEEE Trans Med Imaging.* 2010:29(1): 196-205
[18] Shamonin DP, Bron EE, Lelieveldt BPF, Smits M, Klein S, Staring M. Fast Parallel Image Registration no CPU and GPU for Diagnostic Classification of Alzheimer's Disease. *Front Neuroinform*. 2014:7(50): 1-15
[19] van der Meulen P, Groen JP, Cuppen JJ. Very fast MRI by field echoes and small angle excitation, *Magn Reson Imaging*. 1985:3(3):297-9.
[20] van der Meulen P, Groen JP, Tinus AM, Bruntink G. Fast field echo imaging: an overview and contrast calculations. *Magn Reson Imaging*. 1988:6(4):355-68.
[21] Lagarias JC, Reeds JA. Convergence Properties of the Nelder-Mead Simplex Method in Low Dimensions. *SIAM J. Optim*. 1998:9(1):112-147.
[22] Chen CC, Wan YL. Quality Assurance of Clinical MRI Scanners Using ACR MRI Phantom: Preliminary Results. *J Digit Imaging*. 2004:17(4):279-84.
[23] Baldwin LN, Wachowicz K. Characterization, prediction, and correction of geometric distortion in 3T MR images. *Med Phys*. 2007:34(2):388-99.
[24] Wang D, Doddrell DM. A novel phantom and method for comprehensive 3-dimensional measurement and correction of geometric distortion in magnetic resonance imaging. *Magn Reson Imaging*. 2004:22(4):529-42.
[25] Soliman A, Chugh B. Evaluation of a New MR-Compatible Respiratory Motion Device at 3T. *Med Phys*. 2016:43(6):3389-90
[26] Czervionke LF, Daniels DL, Wehrli FW, et al. Magnetic susceptibility artifacts in gradient-recalled echo MR imaging. *AJNR AM J Neuroradiol*. 1988:9(6):1149-55.

[27] Mann P, Witte M, Moser T, et al. 3D dosimetric validation of motion compensation concepts in radiotherapy using an anthropomorphic dynamic lung phantom. *Phys Med Biol*. 2017:62(2):573-595.
[28] Ehrbar S, Perrin R, Peroni M, et al. Respiratory motion-management in stereotactic body radiation therapy for lung cancer – A dosimetric comparison in an anthropomorphic lung phantom (LuCa). *Radiother Oncol*. 2016:121(2):328-334.